Computer simulations of structures and properties of the biomaterial hydroxyapatite

N. H. de Leeuw*[ab]

Received 15th October 2009, Accepted 27th January 2010
First published as an Advance Article on the web 5th March 2010
DOI: 10.1039/b921400c

Carbonated hydroxyapatite is the major mineral phase in natural bone and teeth and is therefore an attractive material for use in tissue replacement applications. However, its successful application as a biomaterial requires a detailed understanding of its bulk and surface structures, defect chemistry, growth and dissolution behaviour and interaction with complex biomolecules. Computer modelling can aid experiment by investigating at the atomic level highly complex structures, properties and processes, which are still difficult or impossible to access with experimental techniques. Here, we describe our use of a combination of complementary computational techniques to investigate a number of topical issues relevant to the use of hydroxyapatite in biomaterials applications, including the bulk and surface structures of the pure material; the structure and location of carbonate impurities in the lattice; the uptake of fluoride and its effect on hydroxyapatite dissolution; and crystal growth inhibition by citric acid.

1. Introduction

Apatites $Ca_{10}(PO_4)_6(F,Cl,OH)_2$ are a complex and diverse class of materials, which are becoming increasingly important as candidates for use as biomaterials. Carbonated hydroxyapatite (HA) is the main mineral phase of mammalian tooth enamel and bone,[1] where it grows as nano-sized mineral platelets at nucleation sites on a protein template.[2,3] The apatite platelets, with average lengths and widths of 50 × 25 nm,[4] are very thin indeed, typically 2–4 nm,[3] and these crystallites are arranged in an ordered fashion within and around collagen fibrils, where the apatite mineral is aligned with its c-axis, the [0001] direction, along the fibril.[2,4]

Due to its importance as a natural bone mineral, synthetic hydroxyapatite is often used as a bio-active material in biomedical applications, for example as a coating for surgical implants or in glass-ceramic composites for dental applications.[5] However, depending on the composition (substitutions and formation of other calcium phosphates), the porosity of the sample, and the grain size of the hydroxyapatite obtained during the synthetic processes, the behaviour of apatite-like materials may vary from being very soluble, *i.e.* a biomaterial that would be able to be absorbed by the body, to bioinert, *i.e.* a material which will present a very low biological activity. It is clearly of interest to these biomedical applications of the apatite material that we gain a clear understanding of the structural and defect properties of hydroxyapatite and processes affecting the mineral growth.

Natural hydroxyapatite is rarely found as a pure phase. In a geological environment, apatite is often found as a solid solution of fluor-, chlor- and hydroxyapatite,[6,7] also containing a range of cation impurities, such as lanthanide and actinide ions.[8,9] Over the last decades, the prevention of caries in tooth enamel has been sought through strengthening its hydroxyapatite mineral phase through the incorporation of fluoride, to which end fluoride was introduced in tooth paste and drinking water.[10] The strengthening of the hydroxyapatite is thought to be due to the replacement of hydroxy groups by fluoride ions in the hydroxyapatite structure, hence promoting the formation of the less soluble fluorapatite variation,[11] although redeposition of dissolved hydroxyapatite as less soluble fluoridated species may be even more important.

As mentioned, hydroxyapatite in natural bone and tooth enamel also contains a significant proportion of calcite $CaCO_3$,[1]

[a]*Department of Chemistry, University College London, 20 Gordon Street, London, WC1H 0AJ, UK. E-mail: n.h.deleeuw@ucl.ac.uk*
[b]*Institute of Orthopaedics and Musculoskeletal Science, University College London, Brockley Hill, Stanmore, Middlesex, HA7 4LP, UK*

N.H. de Leeuw

Nora de Leeuw obtained her PhD in Computational Materials Chemistry from the University of Bath in 1997. After further postdoctoral research in Bath and a lectureship at the University of Reading, she was awarded an EPSRC Advanced Research Fellowship in 2002 to work in Birkbeck College, University of London on the Computer Modelling of Biomaterial Interfaces. In 2006 she moved to University College London, where she was promoted to Professor of Computational Materials Science in 2007. Her research in computational materials chemistry includes properties of composite biomaterials, catalytic science and geochemistry, in particular CO_2 conversion and sequestration.

and carbonate defects are therefore an important consideration in biological samples. Apatites with up to 5–6% CO_3^{2-} and less than 1% fluoride are often referred to as dahllite and due to the appreciable content of carbonate rather than fluoride in bone and tooth enamel, the apatite mineral present in bone is therefore sometimes also referred to as dahlite. In dental enamel, the hydroxyapatite crystals are found as prisms or rods made up of dense hydroxyapatite clusters of dimensions relatively bigger than those in bone,[1] with appreciable amounts of fluoride, magnesium and carbonate impurities. The presence of these carbonate impurities in hydroxyapatite alters the physical and chemical properties of the material and it has been shown that a higher carbonate content is associated with a smaller grain size, a reduction in crystallinity and an increase in the extent of dissolution of apatites.[12–16]

Computational methods are well placed to investigate, often at the atomic level, the highly complex apatite structures and properties as well as physico-chemical processes involving these minerals, which are still difficult or impossible to access with experimental techniques. Even so, atomistic simulation studies of hydroxyapatite are relatively recent, initially concentrating on the pure material,[17–20] including the relationship between the disordered hexagonal and ordered monoclinic phases,[21,22] and, more recently, the structures and properties of surfaces.[23–28] Defect calculations have also been carried out on a range of impurity ions in the hydroxyapatite lattice, including anionic and cationic species substituting for hydroxy and phosphate groups[29–31] and calcium ions,[32–34] respectively, as well as lattice vacancies[35–37] and neutral interstitial species such as carbon dioxide and water.[35,38]

Two major areas, which have been the subject of extensive computational research, are the mechanical properties of hydroxyapatite and its interface with proteins and peptides, insight into both of which is important for the design and improvement of hydroxyapatite-based materials for bio-medical applications. The latter topic has been investigated primarily with large-scale Molecular Dynamics simulations, *e.g.*,[39–46] although with the unprecedented growth in computing power over the last decades, electronic structure calculations are increasingly used to investigate the adsorption of water and small organic adsorbates to the hydroxyapatite surfaces.[26,27,47,48] Often simulations have focussed on the adsorption of important peptides and proteins,[49,50] for example collagen[46,51,52] which is the major protein phase in bone and understanding its interaction with hydroxyapatite is thus of prime importance. The mechanical properties of hydroxyapatite and HA composites have been investigated computationally using a range of different techniques, from quantum mechanical calculations[53,54] and forcefield-based simulations[35,55–57] to finite element[58–63] and coarse-grained methods.[64,65] These applications of a variety of techniques show very nicely how we can obtain desired information most comprehensively through an informed choice of relevant and often complementary techniques to study different aspects of the same material.

In the present paper, we describe our use of a combination of complementary computational techniques to investigate at the atomic level a number of topical issues relevant to the use of hydroxyapatite (HA) in biomaterials applications, *i.e.* whether we can identify any ordering of hydroxy groups, as implied by pure synthetic samples, but not observed in the natural material; the incorporation of carbonates and fluoride in the HA structure and their effect on the material's structure and dissolution behaviour; and finally, the effect of citric acid on surface growth and morphology.

2. Computational methodology

The approach we have used is to employ quantum mechanical calculations based on the Density Functional Theory (DFT) to study applications, where electron transfer processes and chemical bonding is important, coupled with interatomic-potential methods, including energy minimisation and Molecular Dynamics simulations (MD), to investigate larger-scale and multi-phase systems, for example surface-adsorbate systems in an aqueous environment.

Planewave pseudopotential DFT techniques as used here have become a generally accepted method for applications in the materials sciences, although they have certain limitations. The electron density can become too delocalised, leading to bandgaps which are too small and in extreme cases showing metallic behaviour in insulator materials. However, whereas this has been shown to be a real issue in materials containing transition metals, *e.g.*,[66,67] leading to the development of new methodology to localise d- and f-electrons, it has not been a problem in the closed-shell hydroxyapatite material. Another failure of DFT is its inability to model dispersive forces properly, which are especially important when we consider semi-covalent systems or interactions with organic adsorbates, where van der Waals forces play an important role.[68] In this work, the DFT calculations have only been used for the hydroxyapatite material itself, which is primarily an ionic material where dispersive forces are insignificant compared to the electrostatic interactions and good agreement is obtained between calculated results and experimental data, where available. An excellent review of the strengths and weaknesses of modern DFT methods is given by Neyman and Illas.[69]

Methods based on forcefields can model the van der Waals forces accurately as the interatomic potential parameters include these interactions explicitly. As such, they are better suited for the modelling of covalent systems such as proteins and polymers. However, they are not capable of modelling electronic properties or chemical processes where bond breaking and making is important, such as proton transfer and chemisorption. Thus, they are often used for the determination of structural and mechanical properties, *e.g.* surface geometries and elastic constants, and physical processes such as diffusion and physisorption. Accurate forcefields, carefully derived against a range of relevant experimental and/or calculated data, often generate highly accurate data which agree to within a few percent with experiment and *ab initio* results.[70]

2.1 Density functional theory calculations

For the electronic structure calculations, we have determined the total energies and geometries of the hydroxyapatite structures using the Vienna Ab Initio Simulation Program (VASP),[71–74] employing ultra-soft pseudo-potentials which allow a smaller basis set for a given accuracy.[75,76] Within the pseudo-potential

approach only the valence electrons are treated explicitly and the pseudo-potential represents the effective interaction of the valence electrons with the atomic cores. The valence orbitals are represented by a plane-wave basis set, in which the energy of the plane-waves is less than a given cutoff (E_{cut}). The magnitude of E_{cut} required to converge the total energy of the system has important implications for the size of the calculation when studying elements such as oxygen, which has tightly bound 2p electrons. In our calculations the cores consisted of orbitals up to and including the 1s orbital for both oxygen and fluorine, the 2p orbital for phosphorus and the 3s orbital for calcium (H has no core). As the Ca 3p orbitals have an explicit influence on the valence shell properties, they are calculated directly together with the 4s valence electrons. The calculations were performed within the generalized-gradient approximation (GGA), using the exchange–correlation potential developed by Perdew *et al.*[77] The degree of convergence of the total energy depends on a number of factors, two of which are the plane-wave cutoff and the density of k-point sampling within the Brillouin zone, which were set on the basis of a number of test calculations at a value for E_{cut} of 500 eV and a 2 × 2 × 2 Monkhorst–Pack k-point mesh,[78] so that the total energy is converged to within 0.03 eV (<0.01%) and the lattice parameters to within 1.5% of the experimental lattice parameters.

These DFT calculations were static energy minimisations, which do not take into account temperature, in effect modelling the system at 0 K without the zero-point energy. The optimisation of the atomic coordinates (and unit cell size/shape for the bulk materials) was performed *via* a conjugate gradients technique which utilises the total energy and the Hellmann–Feynman forces on the atoms (and stresses on the unit cell). The calculations of the pure and substituted hydroxyapatite structures were performed on equivalent supercells to achieve cancellation of basis set errors. When calculating the energies of the different locations of the hydroxy groups and the substitutional fluoride and carbonate ions in the lattice, we have investigated a range of different configurations to ensure that as far as possible the lowest-energy configuration was obtained.

2.2 Interatomic potential simulations

For the larger simulations of the substituted hydroxyapatite structures and surfaces in aqueous solution, we have employed the less computationally intensive atomistic simulation techniques, both static energy minimisations and Molecular Dynamics (MD) simulations, where the simulated systems are described by a set of interatomic potential parameters. The energy minimisation code METADISE[79] has been used to derive the interatomic potential model for the hydroxyapatite material and its interactions with impurity and adsorbate species, and to investigate the incorporation of fluoride and carbonate in the bulk hydroxyapatite structure. For the MD simulations of the surface systems, we have employed the DL_POLY code[80] to investigate the systems at constant pressure and a temperature of 310 K, which fluctuated by less than 10 K during the data collection runs of at least 500 ps each. The integration algorithms in DL_POLY are based around the Verlet leap-frog scheme[81] and we have used the Nosé–Hoover algorithm for the thermostat,[82,83] as this algorithm generates trajectories in both NVT and NPT ensembles, thus keeping our simulations consistent. The Nosé–Hoover parameters were set at 0.5 ps for both the thermostat and barostat relaxation times. Following conventional MD simulation procedures with three-dimensional periodic boundary conditions, the surface simulation cells consisted of (2 × 2 × 3) slabs of hydroxyapatite crystal (approximately 20 Å thick) with surfaces on either side, separated by a gap of 50 Å from its images in the neighbouring cells, which is filled by water molecules.

2.2.1 Interatomic potential model. Interatomic potential (IP) methods are based on the Born model of solids,[84] which assumes that the ions in the crystal interact *via* long-range electrostatic forces and short-range forces, including both the repulsions and the van der Waals attractions between neighbouring electron charge clouds, which are described by simple analytical functions. The electronic polarizability of the ions is included *via* the shell model of Dick and Overhauser,[85] where each polarizable ion, in our case the fluoride ions and the oxygen ions in the apatite crystal and water molecules, is represented by a core and a massless shell, connected by a spring. The polarizability of the model ion is then determined by the spring constant and the charges of the core and shell. When necessary, angle-dependent forces are included to allow directionality of bonding, for example in the covalent phosphate anion.

The simulations highlighted in this paper required the development of an extensive suite of compatible potential models for the description of the interactions of the numerous atoms in the simulated apatite systems, including interatomic potential parameters for the pure hydroxyapatite crystal and its interactions with substitutional fluoride and carbonate ions and water in the solvent.[9,31,86–88] The established CVFF forcefield[89] was used for the simulations of the organic adsorbate molecules, but new parameters were required for the description of their interactions with the hydroxyapatite crystal and water.[24,90]

2.3 Hydroxyapatite structure

Hydroxyapatite has a hexagonal structure with spacegroup $P6_3/m$, where the experimental dimensions of the unit cell of the pure material are reported to range from $a = b = 9.398$ Å to 9.438 Å and $c = 6.868$ Å to 6.887 Å, with $\alpha = \beta = 90°$ and $\gamma = 120°$.[91–94] The crystal structure, shown in Fig. 1 as plan and side views with respect to the (0001) basal plane, is built up of a framework of PO_4 tetrahedra, where two oxygen atoms are located on a horizontal plane (with respect to the c-axis) and the other two are positioned on an axis parallel to the c-direction. Within the unit cell the PO_4 tetrahedra are situated in two layers, at a height of 1/4 and 3/4 of the unit cell respectively, and distributed in such a way that they form two types of channels perpendicular to the basal plane.[95] The first type has a diameter of 2 Å and is occupied by calcium ions Ca(I), where each unit cell contains two channels with two calcium ions each at heights of 0 and 1/2 of the unit cell. The second type of channel (diameter = 3–3.5 Å) has its walls formed by oxygen atoms and by Ca(II) ions, located at heights of 1/4 and 3/4, which constitute two equilateral triangles perpendicular to the c-axis, offset from each other by a rotation of 60°. As a result, the overall shape of this second type of channel is hexagonal and it is here that the hydroxy groups are

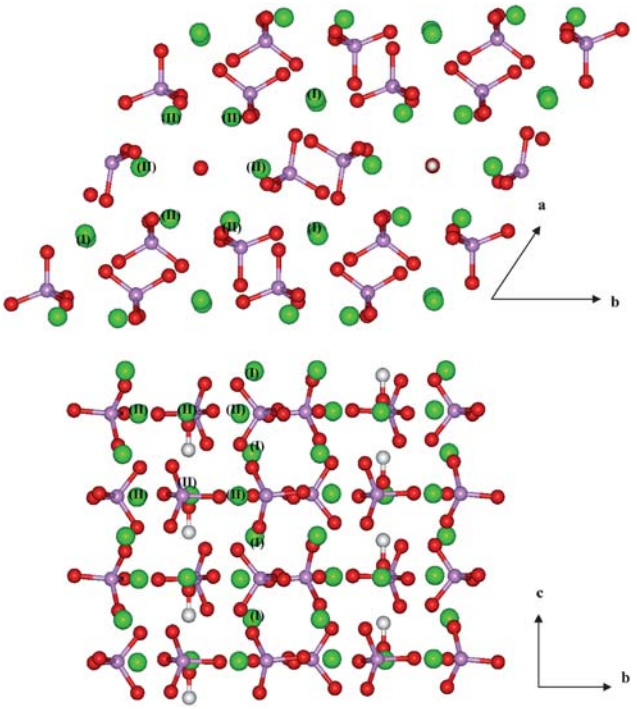

Fig. 1 Plan and side views of the hydroxy apatite structure, showing the hydroxy groups in hexagonal channels surrounded by Ca ions in the Ca(II) positions, where the Ca(I) positions are within the rest of the lattice (O = red, Ca = green, P = pink, H = white, Ca(I) and Ca(II) indicated on some positions).

located in hydroxyapatite, although different anions (O,F,Cl) or impurities can be found in these channels as well.[35,38]

2.3.1 Surface simulations. The (0001) basal plane, which is perpendicular to the hexagonal hydroxy channels in the c-direction, is thermodynamically the most stable apatite surface[86] and widespread in the geological environment.[6] The $(01\bar{1}0)$ surface, with the hydroxy channels lying parallel to the surface, is thermodynamically less stable than the basal plane,[24,48,90] but nevertheless it is the most important surface in biological hydroxyapatite, for example in the mineral platelets in bone, which grow from a collagen template.[96] Thus, because both (0001) and $(01\bar{1}0)$ surfaces are important in hydroxyapatite morphologies, we have considered both surfaces in our simulations. When the surfaces are created from the bulk crystal, the PO_4 groups are kept intact, as they act as molecular poly-anions, similar to the hydroxy groups in the structure.[17] The surfaces considered here are perfect planes, without defects such as vacancies, steps or kink sites. Previous calculations have shown that this type of surface usually adsorbs water in an associative fashion, *e.g.*[97,98] and in our surface simulations we have therefore completed the coordination of the surface species by adding several layers of water molecules.

2.3.2 Surface and adsorption energies. The stabilities of the surfaces are quantified by the surface energy, which experimentally is the energy required to cleave the bulk crystal exposing the surface, as given by:

$$\gamma = (E_{surf} - E_{bulk})/A \quad (1)$$

where E_{surf} is the energy of the simulation cell containing the surface, E_{bulk} is the energy of an equivalent number of bulk stoichiometric units and A is the surface area. A low positive value for γ indicates a stable surface. If water is present, there will be an extra term for the energy of the bulk water in eqn (1), in addition to the energy of the bulk mineral, and E_{surf} becomes the total energy of the hydrated surface consisting of both the hydroxyapatite and the water in the simulation cell.

When we investigate the sorption of biomolecules at the hydroxyapatite surfaces, we need to create surface supercells large enough that the adsorbed molecule avoids interaction between itself and its images in neighbouring repeat cells. The strength of interaction of the surface with the adsorbate is calculated as follows:

$$\mathbf{E}_{ads} = \mathbf{E}_{system} - (\mathbf{E}_{surf} + \mathbf{E}_{molecule}) \quad (2)$$

where E_{system} is the energy of the complete system containing the (hydrated) mineral surface and the adsorbed molecule, E_{surf} is the energy of the (hydrated) surface and $E_{molecule}$ is the energy of the isolated (solvated) molecule. A negative adsorption energy thus indicates that adsorption at the surface is thermodynamically favourable.

3. Simulations of the hydroxyapatite bulk crystal

We first describe our simulations of the bulk crystal structure of pure hydroxyapatite (HA). Although pure synthetic HA crystallises in a monoclinic, fully ordered structure, the natural material has a hexagonal structure with disordering found among the hydroxy groups. As we are interested in modelling the natural material found in bones and teeth, we first need to identify the location of the hydroxy groups.

3.1 Local ordering of hydroxy groups

In hexagonal HA, the hydroxy groups are distributed over two sites per hydroxy group, with a partial occupancy of 50%. However, it is not clear from crystallographic studies,[91–95] whether the hydroxy groups are truly disordered, or whether they are ordered into local domains at short range, which would still provide an averaged disordered structure as seen experimentally. The crystallographic symmetry position for the anions (O or F in oxy- or fluorapatite respectively) in the hexagonal channels parallel to the c-axis (Fig. 1) is (0, 0, 0.25), whereas the hydroxy groups in natural HA are located either above or below this symmetry position in the c-direction, O at (0, 0, 0.2008) and H at (0, 0, 0.0617). The deviation of the hydroxy group away from the symmetry position, leading to four possible hydroxy locations in the unit cell, on either side of two symmetry positions, causes the observed disorder of the hydroxy groups. We have shown this arrangement schematically in Table 1.

We have investigated whether the occupancy of the oxygen and hydrogen sites is likely to be completely random or whether we could identify local ordering in domains. To this end, we have calculated four possible configurations for the oxygen and hydrogen ions in HA, shown in Table 1, where for clarity the (Cartesian) symmetry positions are identified together with the

Table 1 The experimental and calculated Cartesian coordinates (c-direction) of four different hydroxy group configurations in the hydroxyapatite structure, together with the calculated total energies

Symmetry Position	Experimental hydroxy sites		Configuration 1		Configuration 2		Configuration 3		Configuration 4	
1.720	H(1)	0.425	H(1)	—	H(1)	0.456			H(1)	0.520
	O(1)	1.382	O(1)	—	O(1)	1.453				
	O(2)	2.059	O(2)	—			O(2)	1.728	O(2)	1.518
	H(2)	3.016	H(2)	—			H(2)	2.722		
5.160	H(3)	3.865			H(3)	3.873	H(3)	4.146	H(3)	3.853
	O(3)	4.822			O(3)	4.871	O(3)	5.140	O(3)	4.851
	O(4)	5.499								
	H(4)	6.456								
Total Energy/eV			Not converged		−311.171		−310.740		−311.175	

hydroxy positions above and below the symmetry position in the c-direction. Table 1 further shows which of the oxygen and hydrogen positions are occupied in the different calculations, with their final coordinates in the c-direction, where the unit cell shown is periodically repeated in three dimensions. In configuration 1, both hydroxy groups are located at the two sites corresponding to one symmetry position, while configurations 2 and 3 have the hydroxy groups located at sites corresponding to both symmetry positions. In configuration 2, all hydroxy groups are lined up with the hydrogen and oxygen ions alternating along the c-axis, whereby each hydroxy group forms one O–H bond of 0.957 Å and one rather long O···H hydrogen-bond of 2.483 Å, while configuration 3 forms a column of pairs of hydroxy groups, with the hydrogen ions pointing towards each other at an initial separation of only 0.849 Å and an O···O separation of 4.117 Å. Finally, in configuration 4 we have investigated whether the oxygen and hydrogen ions of hydroxy groups were likely to be found separated in the apatite structure, by splitting up one hydroxy group into its constituent atoms, whereby the hydrogen atom of the remaining hydroxy group can form a hydrogen-bond to the separated oxygen atom at 1.806 Å, while the separated hydrogen is in a position to form one short and one long hydrogen-bond with the oxygen atoms at 1.634 and 2.483 Å.

After electronic and ionic relaxation, the total energies of the structures are compared (Table 1). We find that starting configuration 1, where two hydroxy groups were located either side of a single symmetry position, did not lead to a stable structure. Configuration 3 led to a stable structure, but the positions of the hydroxy groups had shifted away from the experimental locations by about 0.3 Å to the positions shown in Table 1, due to repulsion between the two neighbouring hydrogen ions, which leads to an increase in the distance between the hydroxy groups of 0.65 Å. The structure has somewhat expanded from the experimental structure in the a- and b-directions to $a = b =$ 9.551 Å and contracted in the c-direction, $c = 6.868$ Å. Configurations 2 and 4 are the most stable structures, with practically identical energies ($\Delta E < 0.4$ kJ mol^{-1}). On inspection of Table 1, we see that the hydrogen and oxygen ions in configuration 2 remain virtually at their initial positions with lengthening of the O–H bond lengths from 0.957 Å to 0.998 Å. The a- and b-vectors increase to $a = b = 9.564$ Å, but contraction occurs again in the c-direction, $c = 6.831$ Å, which causes the apparent shift of the oxygen and hydrogen ions away from their initial position. In configuration 4 ($a = b = 9.563$ Å, $c = 6.832$ Å), the dissociated hydroxy group in the initial structure has recombined upon geometry optimisation, and is located at the same site as in configuration 2, with a final O–H bond length of 0.998 Å, forming a series of hydrogen-bonded interactions down the c-axis at alternating O···H distances of 2.335 and 2.500 Å. If we compare these hydrogen-bonds to configuration 2 (Fig. 2), where we find all O···H interactions down the c-axis at 2.42 Å, it is clear that configuration 2 is a more regular structure even though energetically identical. Contour plots of the electron density in the plane of the hydroxy groups show that the O–H bond has covalent character, but bonding of its oxygen atom to neighbouring calcium ions is fully ionic, as is the interaction between calcium ions and the oxygen atoms of the phosphate groups.[17,99]

Our calculations of different possible configurations of hydroxy groups within the hydroxy-apatite structure have shown that there is a preferred arrangement of the hydroxy groups, where the energetically most favourable configurations (2 and 4) have all hydroxy groups lined up with oxygen and hydrogen ions alternating in a column parallel to the c-axis, as shown in

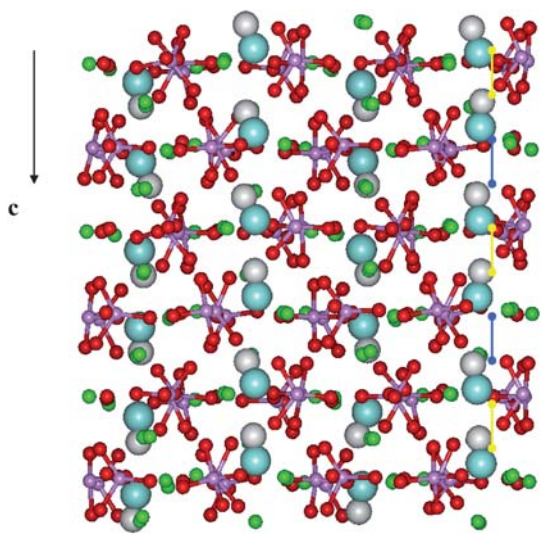

Fig. 2 Side view of the hydroxyapatite structure from MD simulations, showing pairing of the aligned OH groups in the hexagonal channels in the c-direction ($O_{phosphate}$ = red, Ca = green, P = purple, O_{OH} = pale blue, H = white, yellow O···H distance = 2.1 Å, blue O···H distance = 2.8 Å).

Fig. 1(b). When the hydroxy groups have neighbouring oxygen ions (configuration 1) the structure is not stable, while introducing a pair of hydroxy groups with hydrogen ions in neighbouring positions (configuration 3) costs approximately 42 kJ mol^{-1} (0.436 eV/OH pair), and the aligned columns are clearly the most stable arrangement. These columns of aligned hydroxy groups can of course be found in two directions, either up or down the c-axis. However, the difference in energy between a HA crystal where the direction of the hydroxy groups in neighbouring columns alternates, compared to a crystal with the hydroxy groups in all columns pointing in the same direction is negligible at only $\Delta E = 1.3$ kJ mol^{-1}. Hence, we predict that the naturally found hexagonal hydroxyapatite structure consists of local domains of columns with aligned hydroxy groups, but without directional ordering in the hydroxy groups between columns. A change in the ordering of the hydroxy groups between columns is therefore not energetically prohibitive, and may be promoted by the presence of anionic impurities such as F, which we will investigate in section 4 below.

The above DFT calculations were all carried out without taking into account temperature or vibrational properties of the HA crystal. In order to study whether the explicit inclusion of temperature and the evolution of time in the simulations would affect the HA structure, and especially the behaviour of the hydroxy groups in the hexagonal channels, we have also carried out Molecular Dynamics (MD) simulations at 310 K (37 °C), which is body temperature and thus relevant to the application of hydroxyapatite as a biomaterial. We found that during the simulations the hydroxy groups remained lined up within the columns (Fig. 2), in agreement with the DFT calculations above. However, we observe that now the OH···O hydrogen-bond distances alternate between approximately 2.1 and 2.8 Å, shown for one column in Fig. 2 as yellow and blue distances respectively, similar to configuration 4 described in the DFT calculations above (Table 1) but more extreme. It thus appears that the hydroxy groups prefer to exist in pairs, where each pair is closely interacting with its partner, but less so with its other neighbour.[87,88]

4. Impurities in the hydroxyapatite crystal

Having identified a structure for the pure hydroxyapatite crystal, which agrees with both the synthetic and natural structures of the HA mineral observed experimentally, we have next used this model to investigate the incorporation of fluoride and carbonate impurities in the lattice.

4.1 Carbonate defects

Substitutional CO_3 defects in hydroxyapatite are labeled as A- or B-type defects, depending on whether they occupy the OH or PO_4 sites in the HA structure, respectively. Strong evidence for both A- and B-type carbonate defects is provided by a variety of experimental techniques: X-ray diffraction, Fourier transform infra-red spectroscopy (FTIR),[100] electron paramagnetic resonance (EPR) and electron-nuclear double resonance (ENDOR),[101] nuclear magnetic resonance (NMR)[14,102] and neutron-scattering.[103] Studies on tooth enamel and apatites synthesized at high temperatures have identified carbonate groups located in the hydroxy channels, replacing the hydroxy ions, leading to an increase in the a-parameter of the apatite lattice,[13,104] whereas substitutional carbonate groups in phosphate locations were observed in human bone mineral[102] and again in high-temperature synthetic apatites,[101,102,105,106] which was accompanied by a shrinkage in the a-parameter of the lattice due to its smaller size.[107,108] Many structural determinations of hydroxyapatite have in fact observed a mixture of these two carbonate defects within the same lattice,[14,104,109,110] as well as a mixture of carbonate and other defects, for example HPO_4^{2-} species,[12,16,111] hydroxy deficiency[12] and a low calcium content.[111,112]

We have calculated the structures and replacement reactions for a series of A- and B-type carbonate defects in hydroxyapatite, using both DFT and interatomic potential techniques, including Molecular Dynamics simulations of the A-type defect to investigate the carbonate ion's mobility in the channel.[31,35,38] The task of identifying the most stable site for carbonate substitution is complicated by the large number of possible positions, orientations and concentrations of the carbonate ions, different charge compensation schemes, and reference states of the reactants and products. For example, static energy minimisation calculations of carbonate substitutions in a (1 × 2 × 2) supercell of hydroxyapatite favour the A-defect, when two of the eight channel hydroxide ions are replaced by one carbonate (Fig. 3), over the B-defect, when phosphate groups are replaced by carbonates at the same site and charge-compensated by calcium vacancies, mono-valent cations or interstitial hydroxy groups.[31,35] However, DFT studies of smaller (1 × 1 × 1) simulation cells have found that the B-defect is energetically preferred when two phosphate ions are replaced by two carbonate ions with the creation of a calcium vacancy compared to a cell where all hydroxy groups are replaced by carbonate groups,[28,38] indicating that concentration may have a significant effect on the energetics of defect incorporation.

For the DFT calculations of the A-type defect, we have replaced two hydroxy groups with one carbonate ion in a (1 × 1 × 1) simulation cell of the hexagonal HA structure, *i.e.* a complete column of hydroxy groups has been replaced by carbonate groups. Each oxygen atom of the channel carbonate ion becomes coordinated to two calcium ions with distances of about 2.4 Å, with the six calcium ions forming an approximate octahedron around the carbonate ion. The plane of the carbonate ion lies almost perpendicular to a line between the oxygen atoms of two phosphate ions which are slightly closer to the carbonate ion than the other four.[38] The structure of this carbonate defect from our

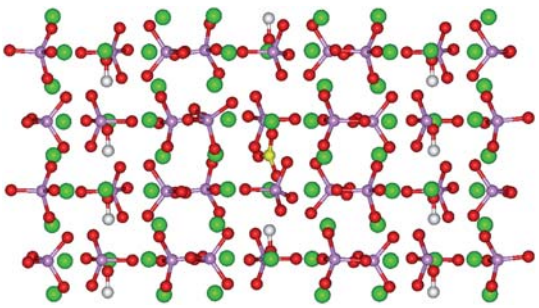

Fig. 3 Side view of the lowest energy HA structure with A-type carbonate defect replacing half the hydroxy groups in one hexagonal channel (O = red, Ca = green, P = pink, H = white, C = yellow).

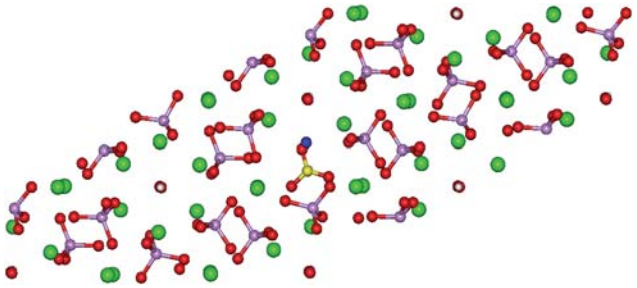

Fig. 4 Plan of the lowest energy hydroxyapatite structure with B-type carbonate defect, created by replacing a PO_4^{3-} group by a CO_3^{2-} group and one Ca^{2+} ion by a Na^+ ion (O = red, Ca = green, Na = blue, P = pink, H = white, C = yellow).

Table 2 Calculated cell parameters for different B-type carbonate substitutions in hydroxyapatite

Structure	Cell parameters
$Ca_9Na(PO_4)_5(CO_3)(OH)_2$	$a = 16.57$ Å $b = 6.87$ Å $c = 19.11$ Å $\alpha = 90.0°$ $\beta = 151.0°$ $\gamma = 90.0°$
$Ca_{10}(PO_4)_5(CO_3)(OH)_3$	$a = 16.57$ Å $b = 6.92$ Å $c = 19.30$ Å $\alpha = 89.9°$ $\beta = 150.5°$ $\gamma = 90.0°$
$Ca_9(PO_4)_4(CO_3)_2(OH)_2$	$a = 16.38$ Å $b = 6.89$ Å $c = 18.88$ Å $\alpha = 90.0°$ $\beta = 150.5°$ $\gamma = 90.0°$

DFT calculations is very similar to the interatomic-potential simulations of a larger (2 × 1 × 2) unit cell, where carbonates replace half the hydroxy groups in one out of two channels (Fig. 3).[31] When we apply MD simulations to this structure, we find that at body temperature (310 K) the carbonate group rotates freely about the c-axis in the a/b-plane of the HA structure, but only occasionally inverts along the c-axis. The presence and dynamic nature of the carbonate impurity leads to a change in the HA cell parameters (a,b-parametes +0.02%, c-parameter +0.01%),[31] in excellent agreement with experiment.[13,104,107,108]

To investigate B-type carbonate defects, starting structures were created by substituting carbonate for phosphate and balancing the charge by either replacing a calcium ion with a sodium ion, shown in Fig. 4, adding a hydroxy ion, or by creating a calcium vacancy for a pair of carbonate replacements. On relaxation the carbonate ion adopts a planar conformation causing only small structural changes in the HA structure (Table 2).[38]

4.1.1 Reaction energetics. The reaction enthalpies from the DFT calculations for a number of substitutions of aqueous carbonate into HA are as follows:

$$Ca_{10}(PO_4)_6(OH)_{2(s)} + CO_3^{2-}{}_{(aq)} \rightarrow Ca_{10}(PO_4)_6(CO_3)_{(s)} + 2OH^-{}_{(aq)} \quad \Delta H = 48 \text{ kJ mol}^{-1}$$

$$Ca_{10}(PO_4)_6(OH)_{2(s)} + CO_3^{2-}{}_{(aq)} + Na^+{}_{(aq)} \rightarrow Ca_9Na(PO_4)_5(CO_3)(OH)_{2(s)} + Ca^{2+}{}_{(aq)} + PO_4^{3-}{}_{(aq)} \quad \Delta H = 56 \text{ kJ mol}^{-1}$$

$$Ca_{10}(PO_4)_6(OH)_{2(s)} + CO_3^{2-}{}_{(aq)} + OH^-{}_{(aq)} \rightarrow Ca_{10}(PO_4)_5(CO_3)(OH)_{3(s)} + PO_4^{3-}{}_{(aq)} \quad \Delta H = 39 \text{ kJ mol}^{-1}$$

$$Ca_{10}(PO_4)_6(OH)_{2(s)} + 2CO_3^{2-}{}_{(aq)} \rightarrow Ca_9(PO_4)_4(CO_3)_2(OH)_{2(s)} + Ca^{2+}{}_{(aq)} + 2PO_4^{3-}{}_{(aq)} \quad \Delta H = 223 \text{ kJ mol}^{-1}$$

Clearly, all calculated replacement processes are energetically unfavourable, which is not surprising as we are introducing defects into the perfect HA lattice. However, these defects are observed experimentally and from our calculations we would therefore suggest that the substitution of hydroxy groups by carbonate (A-type defect) and replacement of phosphate groups (and Ca) by carbonate and hydroxy groups or carbonate and sodium (B-type defects) are the most likely processes to occur, also taking into account that entropic effects may affect the reaction directions. However, the creation of a Ca vacancy through the replacement of two phosphate groups by two carbonates is so endothermic, even taking into account that twice the number of phosphates are replaced, that we do not expect this process to occur to any significant extent. Our calculations thus suggest that, depending on concentration, we may expect both A-type and B-type carbonate defects to a similar extent, but only when charge-compensating ions are available to stabilise the B-type defect.

4.2 The incorporation of fluoride in hydroxyapatite

Again, we have used both DFT and interatomic potential calculations to study fluor-hydroxyapatite (FHA) solid solutions, where the excess heats of the solid solution $Ca_{10}(PO_4)_6(OH)_{2-x}F_x$ are calculated with respect to the pure fluor- and hydroxyapatite end members as follows:

$$\Delta E_x(FHA) = E(HA_{1-x}FA_x) - \{[1 - x]E(HA) + xE(FA)\} \quad (3)$$

where x is the fraction of hydroxy groups replaced by fluoride ions. Using relevant supercells when required, the calculated excess heats of solid solution are shown in Fig. 5, for the DFT and IP simulations. The computationally less intensive IP simulations gave us the opportunity to use larger supercells and thus sample a more extensive set of configurations for the FHA solid solutions. We first note that the results for the two methods are very similar, both in trend where $x = 0.5$ is the most energetically favourable solid solution of fluor- and hydroxyapatite,

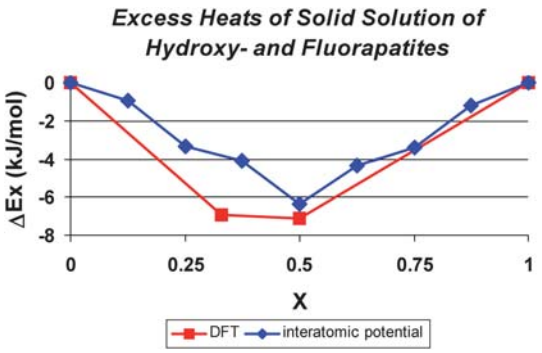

Fig. 5 Graph of the excess heats of solid solution of fully geometry optimized fluor- and hydroxy-apatite, showing DFT calculations of (1 × 1 × 2) and (1 × 1 × 3) supercells (red curve), and interatomic potential calculations of (2 × 2 × 2) supercells (blue curve).

and in actual energy, where $\Delta E_{0.5} = -7.15$ kJ mol^{-1} for the DFT calculation[113] and $\Delta E_{0.5} = -6.35$ kJ mol^{-1} for the interatomic potential calculation.[88] The FHA solid solution is clearly more stable than the individual end-members, with highly stable structures at $x = 0.33$ and $x = 0.50$, shown in Fig. 6(a) and (b) respectively. (The DFT structure at $x = 0.33$ was not repeated by the IP methods).

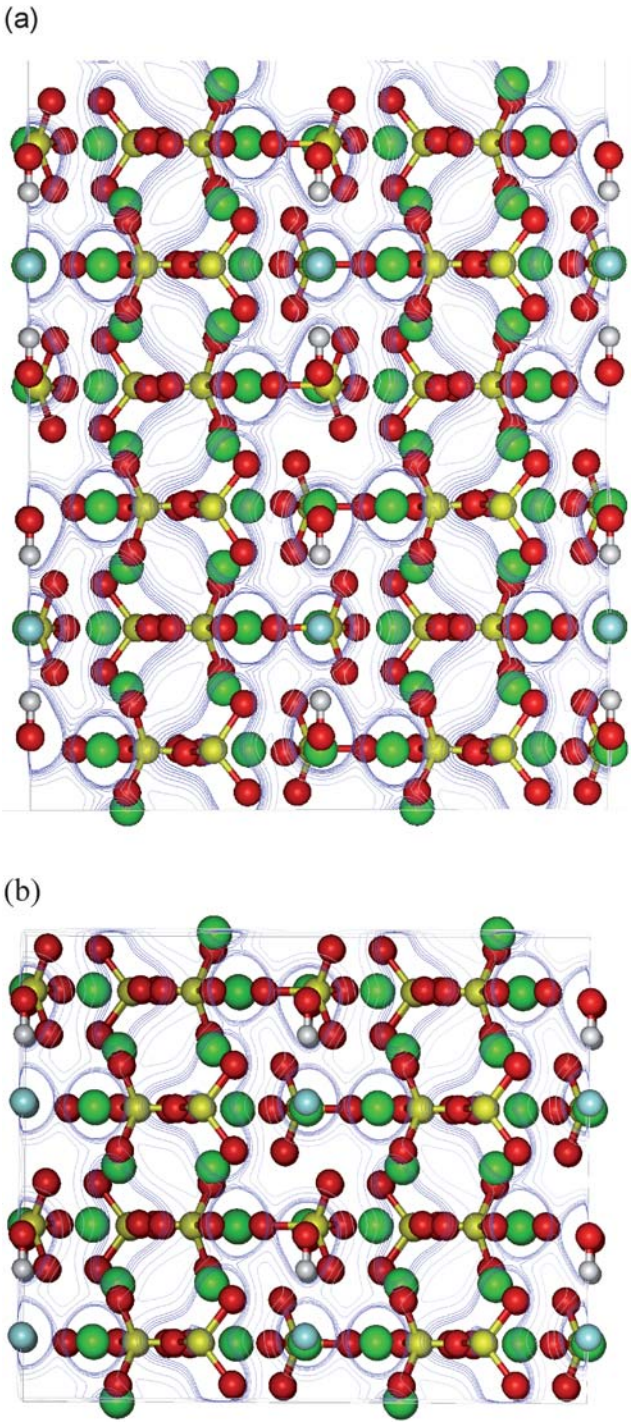

Fig. 6 DFT optimised structure of hydroxyapatite with (a) one third of the hydroxy groups substituted by F ions, where the alignment of the hydroxy groups is reversed in the channel to form strong F···H interactions, and (b) with one half of the OH groups substituted by F ions, where all OH are aligned in the same direction parallel to the c-vector (O = red, Ca = green, P = yellow, F = pale blue, H = white, contour levels from 0.05 to 0.35 eÅ^3 at 0.05 eÅ^3 intervals).

The lowest-energy $x = 0.33$ solid solution, shown in Fig. 6(a), has a configuration where the hydroxy groups neighbouring the F ions are reversed in the hexagonal column in the c-direction in order to form strong H···F interactions between the F ions and hydroxy groups. The fluoride ion in this substituted structure remains at the symmetry site, while the electron density contour plots show that the charge density around the fluoride ions is distorted from a spherical distribution towards both hydrogen atoms. The process is exothermic with respect to the lowest energy structure of pure hydroxyapatite (with all hydroxy groups aligned in the channel), releasing -10.4 kJ mol^{-1} per hydroxy group. However, when we compare the substituted structure, which contains two reversions in the alignment of the hydroxy groups in the simulation supercell, with the pure hydroxyapatite structure containing the same number of OH reversions (see section 3 above), the process becomes even more exothermic at -52.4 kJ mol^{-1}. Thus the presence of fluoride in the hydroxyapatite lattice induces reversal of the hydroxy groups within channels, rather than its occurrence from one channel to the other as seen in the pure HA structure,[17] hence further promoting the hydroxy disorder observed experimentally in hexagonal HA.

For the $x = 0.5$ solid solution, we have not only considered replacement of hydroxy groups within one column, but have also modelled ($2 \times 2 \times 2$) supercells to investigate the position and distribution of the fluoride ions and hydroxy groups of the mixed systems not only in the c-direction, but also between columns in the a/b-planes. In the lowest-energy configuration, the FHA crystal consists of alternating planes of fluoride ions and hydroxy groups, where the F and OH species are alternating in the c-direction, but are co-located within the a/b-plane, as shown in Fig. 6(b). The reason for the stability of these a/b planes of F or OH ions is largely structural. Fluor- and hydroxyapatite have virtually the same lattice parameters ($a = b = 9.36$ Å in FA, $a = b = 9.42$ Å in HA, $c = 6.88$ Å in FA and HA), unlike for example chlor-apatite, which has considerably larger a- and b-parameters (9.64 Å) but a shorter c-parameter (6.78 Å). The introduction of fluoride in hydroxy locations into the HA crystal therefore does not induce any elastic strain in the host lattice, and thus should be possible.[114] Indeed, if we first consider the introduction of an isolated fluoride ion into a hydroxy column, this is calculated to be just favourable at $\Delta E_x = -0.37$ kJ mol^{-1}, because the substitutional F ion is smaller than the hydroxy group and it is able to interact closely with the hydrogen of a neighbouring hydroxy group within the column at 2.1 Å. When a second fluoride ion is introduced in the lattice, it can go to a number of possible sites, where we have considered three configurations: (i) isolated from the first fluoride ion, (ii) next to the first fluoride ion in the same column, or (iii) in a neighbouring column but in the same plane as the first fluoride ion. In the first case, $\Delta E_x = -0.37$ kJ mol^{-1} again, but when the second fluoride ion is introduced in the next hydroxy site above or below the first F ion in the same column, the excess energy of solid solution is almost neutral at $\Delta E_x = -0.08$ kJ mol^{-1}. Only one of the two fluoride ions can now interact with a hydrogen atom, as the other is neighboured by an oxygen ion on the one site and another fluoride ion on the other, which negates to a certain extent the

favourable interaction of the first fluoride ion. Finally, in the third case, when the second F ion is placed in the same a/b plane but in a neighbouring column $\Delta E_x = -0.91$ kJ mol^{-1}. Obviously, there is a small energetic incentive for the second fluoride ion to be located in a neighbouring hydroxy column in the same a/b plane, which is probably due to two factors. Firstly, the fluorapatite structure is slightly smaller in the a- and b-directions (by 0.06 Å) and hence there will be no elastic strain due to substituting more and more hydroxy groups by F ions in the a/b plane. Secondly, since they are diatomic, the hydroxy groups are located off-centre from the symmetry position in the c-direction, whereas the fluoride ion is located on the symmetry position. As such, if the second fluoride ion is introduced in the same a/b plane, it will be located at the same height in the c-direction as the first ion and will not induce much more strain in the lattice than was due to the first ion, whereas if it is introduced in a different a/b plane, it will induce a second strain. For example, in the $x = 0.5$ configuration where the fluoride ions in neighbouring columns are not in the same a/b plane, the apatite structure has become distorted with $\alpha = 89.99°$ $\beta = 89.99°$ and $\gamma = 120.03°$. However, the energy differences between the different configurations are so small that in practice randomization due to entropy may be expected.

5. Surface studies of hydroxyapatite

Finally, we have extended our bulk and defect simulations to model some of the major HA surfaces, especially the (0001) and (01$\bar{1}$0) surfaces, as these are important in the geological[6] and biological morphology,[115] respectively, and there is experimental evidence that these faces act as the binding site for many anionic species, including small molecules, polymers and anionically modified cell surfaces.[116] In this section, we discuss a number of Molecular Dynamics simulations of the structure, stability and hydration behaviour of these surfaces, the effect of fluoride ions on the dissolution of the surface, and the interaction with citric acid.

5.1 The interface with water

The surface energies of the dehydrated (0001) and (01$\bar{1}$0) surfaces are calculated to be 0.80 J m^{-2} and 1.16 J m^{-2}, respectively, *i.e.* the (0001) surface is more stable and less reactive than the (01$\bar{1}$0) surface. This trend was also found in energy minimisation calculations of the same surfaces,[24] although the surface energies obtained from the MD simulations are somewhat smaller due to the greater flexibility allowed to the lattice ions for relaxation, rotation and reconstruction, through the inclusion of temperature.

It is often found that surface hydration reverses stability trends for different surfaces, where relatively unstable surfaces under dehydrated conditions upon hydration become stabilised to a much greater extent than their already stable counterparts. However, although both hydroxyapatite surfaces under investigation are stabilised when the liquid water is introduced in the simulations, they keep their relative stabilities when hydrated, with calculated surface energies of 0.42 and 0.66 J m^{-2} for the (0001) and (01$\bar{1}$0) surfaces respectively. The fact that the (0001) surface is more stable than the (01$\bar{1}$0) surface in aqueous environment indicates that the more reactive (01$\bar{1}$0) surface should grow more quickly and may well grow out of the thermodynamic crystal morphology altogether, leaving large (0001) planes expressed in the crystal morphology.

The two hydrated surfaces are shown in Fig. 7. Unlike surfaces at the vacuum interface, both surfaces show a regular structure at the interface with the water without significant surface relaxation or reconstruction, due to the termination of the under-coordinated surface species by water molecules.[86] Due to the complex and irregular geometry of the underlying HA surface, in contrast

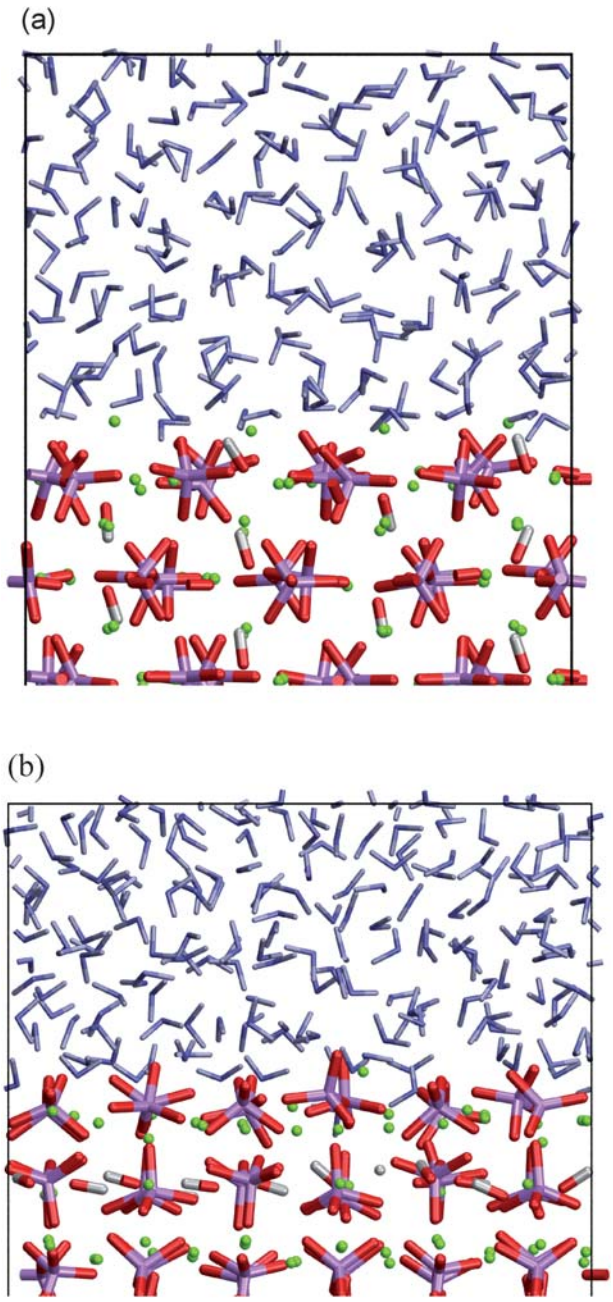

Fig. 7 Average structure of the hydrated hydroxyapatite surfaces from MD simulations (a) the (0001) surface and (b) the (01$\bar{1}$0) surface (O = red, Ca = green, P = pink, H = white, water shown as small blue/white stick models).

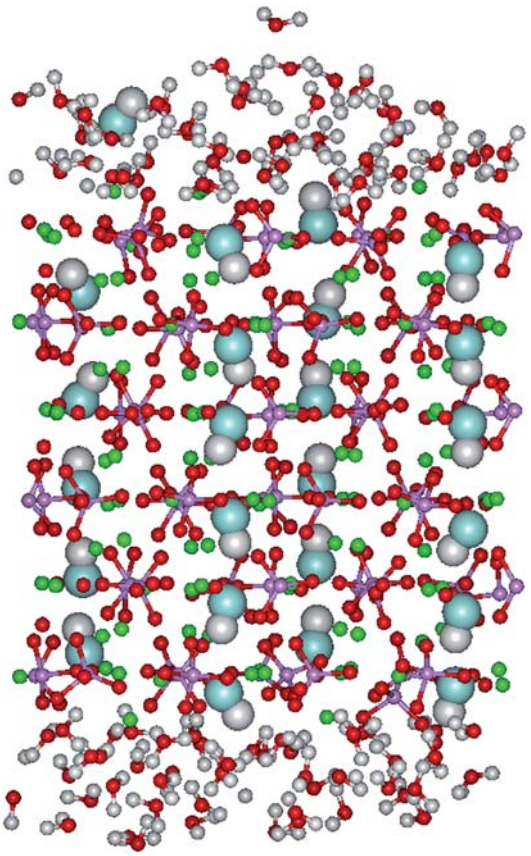

Fig. 8 Side view of the slab of hydroxy-apatite material in water after 100 ps, showing the onset of dissolution of surface hydroxy groups into the solvent water (Ca = green, $O_{hydroxy}$ = pale blue, $O_{phosphate}$ = red, O_{water} = red, H = white, P = purple).

to, for example, simple binary oxide surfaces, the adsorbed water at the interface resembles bulk liquid water without the formation of an ordered overlayer of water molecules.

On the (0001) surface, where the hexagonal hydroxy channels lie perpendicular to the surface plane and are thus easily accessible to the water, we note that during the MD simulations the hydroxy groups in the channels start to diffuse from the channel into the water, as shown in Fig. 8. Although only the hydroxy groups clearly dissolve into the solvent, whereas other surface species remain in the apatite crystal during the length of these MD simulations, the surface calcium ions also show the onset of dissolution to some extent, through lengthening of their bonds to lattice oxygen ions and solvation by surface water molecules.

5.2 The effect of fluoride on hydroxyapatite dissolution

Next we have investigated whether the presence of fluoride affects the onset of dissolution of the HA crystal. We have therefore introduced a fluoride ion at one of the surface hydroxy positions and carried out an identical MD simulation as on the pure crystal surface above. Firstly, we calculated that the substitution of hydroxy groups by F ions from solution into the hydroxyapatite surface is a highly exothermic process, releasing approximately 193 kJ mol^{-1} when the F is located in the surface layer. However, incorporation into the second and third layers is progressively less exothermic, respectively releasing 164 and 68 kJ mol^{-1}, whereas subsequent segregation of fluoride further into the bulk is energetically not particularly favourable beyond approximately 10 Å. Thus, it should be relatively easy to replace surface hydroxy groups by fluoride ions, but the fluoride is not expected to penetrate deeply into the apatite material itself. As a result, whether fluoride is taken up into the hydroxyapatite material through replacement of hydroxy groups or whether FHA is formed through redeposition of dissolved hydroxyapatite material, we can expect only a thin surface layer of fluorinated apatite.

We saw that the onset of dissolution through leaching of surface hydroxy groups was rapid in the pure HA material (Fig. 8). However, the surface fluoride does not dissolve as readily as the hydroxy groups but remains in the HA crystal (Fig. 9). The calculated diffusion coefficient for the surface fluoride ions during the MD simulation is essentially zero (0.00×10^{-9} cm^2 s^{-1}), whereas the diffusion constant for the hydroxy groups in the surface layer only was calculated to be 5.74×10^{-9} cm^2 s^{-1}, which is closer to the average diffusion constant for the water molecules near the surface, *i.e.* 1.50×10^{-7} cm^2 s^{-1}, than for the sub-surface hydroxy groups at 1.23×10^{-12} cm^2 s^{-1}, clearly showing the significant movement of the surface hydroxy groups in solution, similar to the behaviour of a solvated species rather than that of a species confined in a crystal lattice. Moreover, the

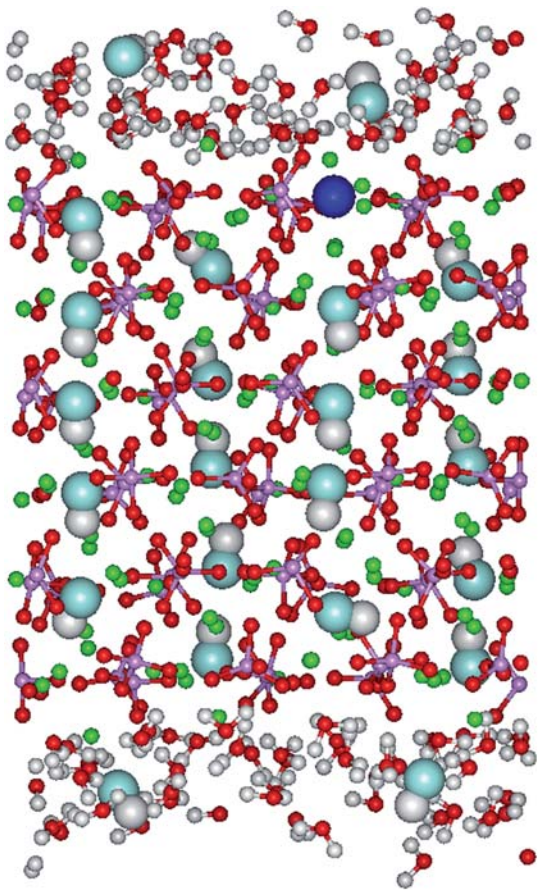

Fig. 9 Side view of the slab of hydroxy-apatite material in water after 500 ps, with one surface OH replaced by a F ion, which remains in the structure while the surface hydroxy groups have dissolved into the solvent water (Ca = green, F = dark blue, $O_{hydroxy}$ = pale blue, $O_{phosphate}$ = red, O_{water} = red, H = white, P = purple).

surface calcium ions, which in the pure HA structure also showed the onset of dissolution, remain more closely coordinated to the material surface in the vicinity of the substitutional fluoride ion in Fig. 9. The incorporation of surface fluoride in the hydroxyapatite material thus has a clear effect on the crystal dissolution and this resistance to dissolution through the incorporation of fluoride is two-fold: (i) the fluoride itself remains in the material structure rather than dissolve from the lattice like the surface hydroxy groups and (ii) it interacts more strongly with the surface calcium ions, binding them to the surface.

5.3 The adsorption of citric acid

We have also investigated the adsorption of citric acid molecules (2-hydroxypropane-1,2,3-tricarboxylic acid $C_6H_8O_7$) at the apatite surfaces. Citric acid derivatives are a class of well known crystal growth inhibitors for hydroxyapatite and other calcium phosphates, including calcium, sodium and phospho-citrates,[117] the latter of which is found as a naturally occurring compound in mammalian mitochondria.[116] In addition, citric acid itself is known to be instrumental in the dissolution of hydroxyapatite tooth enamel,[118] and it can be used as a retardant for the precipitation of calcium phosphate precursor phases.[119]

Fig. 10 shows the citric acid molecule adsorbed at the (0001) and (01$\bar{1}$0) surfaces in the aqueous environment. The citric acid interacts closely with both surfaces, even though it may appear from Fig. 10 that a number of water molecules are closer to the surface than the citric acid. In fact, on the (0001) surface, the first maximum in the O_W–Ca radial distribution function is at 2.47 Å, whereas the first O_{citric}–Ca peak is at 2.28 Å and the second HO_{citric}–Ca peak (from hydroxy groups in the citric acid) a bit further away at 2.52 Å, whereas on the (01$\bar{1}$0) surface the radial distribution functions for O_{citric}–Ca peak at 2.47 Å and for HO_{citric}–Ca at 2.42 Å. As such, the citric acid is more closely bound to the surfaces than the nearest water molecules.

When we calculate the adsorption energy as the difference in energy between the energy of the complete surface-water-citric acid systems and the sum of the energies of the hydrated surfaces and the solvated citric acid, the calculated adsorption energies are +291.4 kJ mol^{-1} for the (0001) and −17.4 kJ mol^{-1} for the (01$\bar{1}$0) surfaces. Clearly, it is energetically preferred for the (0001) surface to be fully hydrated with the citric acid remaining in the bulk liquid water, rather than to have the citric acid molecule adsorbed at the surface. However, the geometry of the (01$\bar{1}$0) surface matches closely the structure of the citric acid functional groups, and thus offers viable adsorption sites for the citric acid compared to water. Adsorption of the citric acid at the (01$\bar{1}$0) surface is hence energetically favourable compared to hydration of this surface, whereas the match between the surface geometry and citric acid molecular structure is less close on the (0001) surface, where the water therefore competes successfully with the citric acid and its adsorption is energetically unfavourable.

The (01$\bar{1}$0) surface is the less stable of the two surfaces, which will hence grow more rapidly than the (0001) surface. Thus, blocking the (01$\bar{1}$0) surface sites with citric acid will significantly retard growth of the HA crystal, in agreement with experimental studies, which have shown that citrate compounds are found to be excellent inhibitors for both hydroxyapatite nucleation[120] and hydroxyapatite growth.[121]

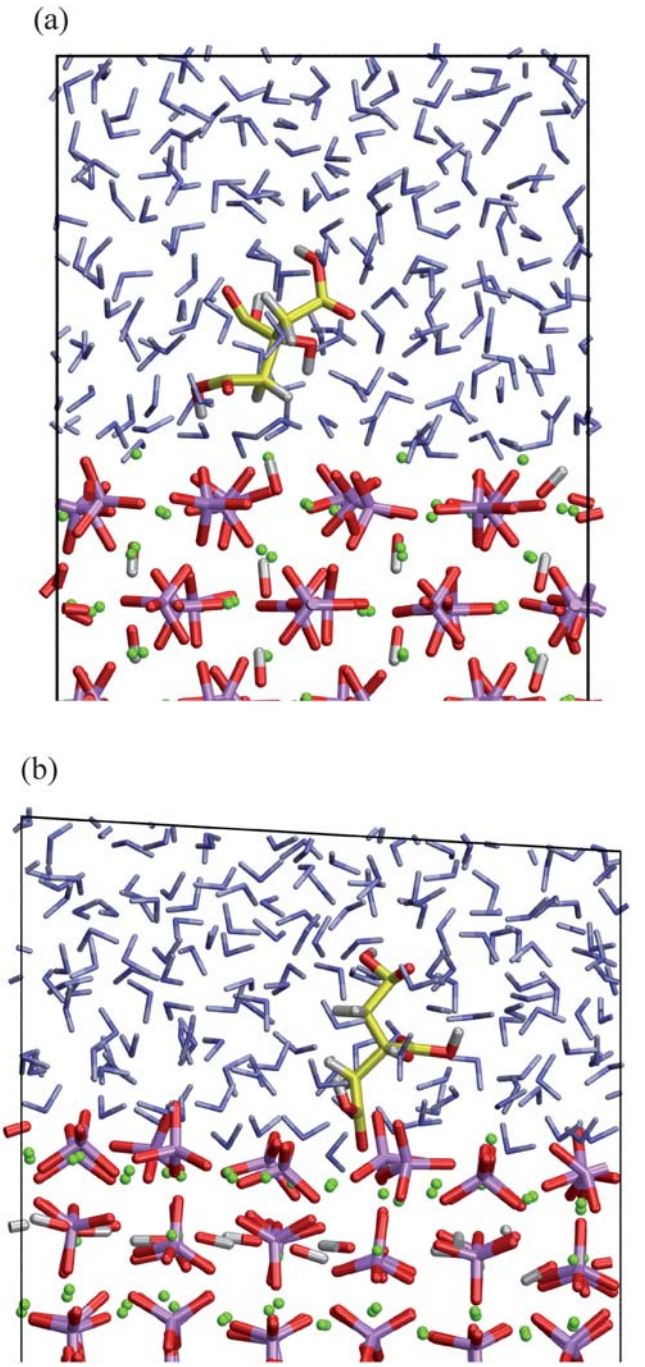

Fig. 10 Average structure of citric acid adsorbed at (a) the (0001) surface and (b) the (01$\bar{1}$0) surface in aqueous environment (O = red, Ca = green, P = pink, H = white, C = gray, water shown as small blue/white stick models).

6. Conclusions

In this paper, we have given an overview of a series of comprehensive computer modelling studies of a number of topical issues in the application of hydroxyapatite as a biomaterial. We have used a powerful combination of Density Functional Theory calculations and classical Molecular Dynamics simulations to investigate the bulk and surface structures of the pure HA

crystal, the incorporation of the common impurities fluoride and carbonate, and the effect of fluoride and citric acid on surface growth and dissolution behaviour.

Our calculations of different possible configurations of hydroxy groups within the hydroxyapatite structure have shown that there is a preferred arrangement of the hydroxy groups, where the energetically most favourable configurations have all hydroxy groups aligned with oxygen and hydrogen ions alternating in a column parallel to the c-axis. These columns of aligned hydroxy groups can of course be found in two directions, either up or down the c-axis, but as the columns do not interact with each other to any significant extent, the calculations predict that the perfect HA structure will consist of local domains of these well-ordered hydroxy columns, thus leading to an average structure with partial occupancies of the crystallographic hydroxy positions, as is observed experimentally. However, when fluoride ions are present in the columns, which is an energetically favourable process compared to the pure fluor- and hydroxyapatite materials, the strong interaction between the fluoride and the hydrogen of neighbouring hydroxy groups can easily lead to reversion of the hydroxy groups within the columns. Similarly, when substitutional carbonate is present in the columns, two of the three oxygens are found almost aligned along the channel in the c-directions, which will interact more strongly with the hydrogens of neighbouring hydroxy groups than their oxygen atoms. Hence, this is another impurity in the HA structure which will encourage reversion of the OH alignment within a single column. Thus, as no HA crystal is compositionally pure, we have shown that the experimentally observed disorder of the hydroxy groups in the natural hexagonal HA structure can be an effect not only of a random distribution between channels of local domains of aligned columns of hydroxy groups, but also of the presence of a number of common impurities in the natural HA material.

Our simulations of the incorporation of carbonate groups in the HA crystal, evaluating a range of different substitution schemes, have shown that the preference for A-type (carbonates in the hexagonal channels) or B-type defects (carbonates replacing phosphate groups) is affected strongly by the particular replacement reaction and charge compensation scheme considered, as well as the defect concentration. As such, depending on the reaction conditions, we would expect both A-type and B-type defects to be feasible, as is indeed found experimentally. Synthetic and high-temperature apatites often contain A-type defects, especially at low carbonate concentrations,[101,122–124] or a mixture of both A- and B-type defects in the lattice,[101,122,123] but B-type defects appear to prevail in natural bone and, to a lesser degree, in tooth enamel.[104,123,125,126] This prevalence of B-type defects in the natural bone mineral may be explained through a mechanism where the carbonate impurities are incorporated at the nucleation phase. The apatitic phase is often formed from calcium phosphate precursor phases, such as octa-calcium phosphate which is structurally similar to apatite in some regions and is thought to exist at the surface of the growing bone apatite before crystallising into hydroxyapatite proper.[125] One feature of these precursor phases is the absence of the hydroxy channels and as such, if carbonate is present in the reaction mixture, it would almost certainly replace phosphate groups in the lattice of the growing material, rather than hydroxy groups which are not as yet part of the crystal lattice.

HA dissolution is shown to be affected by fluoride ions in the crystal surface, which are easily incorporated from solution through cation exchange with rapidly dissolving surface hydroxy groups. They then resist further dissolution of the HA material, through their anchoring of surface calcium groups. However, the fluoride remains at the surface and does not penetrate into the HA crystal, indicating the formation of a fluorinated HA thin film. Our simulations thus agree with experimental findings, where fluoridation of HA is found to harden tooth enamel against dissolution,[10] but where sub-surface fluoridation is only found in lesions in carious enamel.[127]

Finally, investigations of the adsorption of a well-known class of organic HA growth inhibitors have shown that citric acid interacts much more strongly with the HA $(01\bar{1}0)$ surface than the (0001) surface, competing effectively with pre-adsorbed water, indicating that it would effectively inhibit growth of the $(01\bar{1}0)$ surface by binding to surface growth sites. As a result, we expect the $(01\bar{1}0)$ surface to become more pronounced in the hydroxyapatite morphology at the expense of the (0001) surface, which is less affected by the citric acid. The crystal shape of hydroxyapatite grown in the presence of citric acid would thus become elongated along the c-direction of the apatite crystal, with expression of the $(01\bar{1}0)$ surface, as compared to the crystal morphology in the absence of citric acid.

We trust that the above examples of computational investigations of hydroxyapatite material properties and processes have shown how computer modelling at the molecular level can be a valuable tool in the interpretation of experimental data and the prediction of structures and properties, which are not accessible to experimental investigation. With the phenomenal increase in computational power we have seen over the last decades and the availability of large-scale High Performance Computing facilities, we may expect the field of computational biomaterials science to progress rapidly into even more complex materials. As already mentioned, many materials used for biomedical applications are composites to mimic the natural tissue more closely and to improve the performance of the synthetic material. Atomic-level computational techniques are well placed to provide crucial insights into the detailed structural arrangements and the physico-chemical processes taking place at the interface between the constituent phases of the composite materials, where the more compute-intensive quantum mechanical methods will now be able to come into their own. Similarly, classical Molecular Dynamics simulations will be able to model increasingly more realistic systems, including solvent and solvated species at much longer time-scales, whereas coarse-grained methods will benefit from the more accurate input data obtained from these improved models. Increasingly realistic models will also narrow the gap between the data obtained from computation and experiment, such as AFM and other surface science techniques, Raman spectroscopy and NMR, which will lead to better interaction between the respective fields.

7. Acknowledgements

NHdL acknowledges the Engineering and Physical Sciences Research Council, the Natural Environment Research Council, the Medical Research Council, the Wellcome Trust and the Royal Society for funding, and thanks Dr Jeremy Rabone for

useful discussions. Computer resources on the HPC*x* and HECToR services were provided *via* membership of the UK's HPC Materials Chemistry Consortium and funded by EPSRC (portfolio grant EP/D504872 and EP/F067496).

8. References

1 T. S. B. Narasaraju and D. E. Phebe, *J. Mater. Sci.*, 1996, **31**, 1.
2 S. Weiner and H. D. Wagner, *Annu. Rev. Mater. Sci.*, 1998, **28**, 271.
3 P. Fratzl, H. S. Gupta, E. P. Paschalis and P. Roschger, *J. Mater. Chem.*, 2004, **14**, 2115.
4 S. Weiner, T. Arad and W. Traub, *FEBS Lett.*, 1991, **285**, 49.
5 L. L. Hench and S. Best, in *Biomaterials Science: An Introduction to Materials in Medicine*, ed. B. D. Ratner, A. S. Hoffman, F. J. Schoen and J. E. Lemons, Elsevier Academic Press, 2nd Edition, 2004, (ch. 2.10), pp 153.
6 W. A. Deer, R. A. Howie and J. Zussman, in *An introduction to the rock-forming minerals*, Longman, UK, 1992.
7 J. C. Elliott, in *Structure and chemistry of the apatites and other calcium orthophosphates*, Studies in inorganic chemistry 18, Elsevier, 1994.
8 J. Barbarand, A. Carter, I. Wood and T. Hurford, *Chem. Geol.*, 2003, **198**, 107.
9 J. A. L. Rabone and N. H. de Leeuw, *J. Comput. Chem.*, 27, p. 253.
10 D. W. Lewis and D. W. Banting, *Community Dent. Oral Epidemiol.*, 1994, **22**, 153.
11 A. Knappwost, *Angew. Chem.*, 1956, **68**, 371.
12 A. A. Baig, J. L. Fox, R. A. Young, Z. Wang, J. Hsu, W. I. Higuchi, A. Chettry, H. Zhuang and M. Otsuka, *Calcif. Tissue Int.*, 1999, **64**, 437.
13 A. Yasukawa, K. Kandori and T. Ishikawa, *Calcif. Tissue Int.*, 2003, **72**, 243.
14 W. Kolodziejski, *Topics Curr. Chem.*, 2004, **246**, 235.
15 D. G. A. Nelson, J. D. B. Featherstone, J. F. Duncan and T. W. Cutress, *J. Dent. Res.*, 1982, **61**, 1274.
16 R. Z. LeGeros, R. Kijkowska, C. Bautista and J. P. LeGeros, *Connect. Tissue Res.*, 1995, **32**, 525.
17 N. H. de Leeuw, *Chem. Commun.*, 2001, 1646.
18 J. A. Ascencio, V. Rodrigues-Lugo, C. Angeles, T. Santamaria and V. M. Castano, *Comput. Mater. Sci.*, 2002, **25**, 413.
19 S. Hauptmann, H. Dufner, J. Brickmann, S. M. Kast and R. S. Berry, *Phys. Chem. Chem. Phys.*, 2003, **5**, 635.
20 P. Rulis, L. Ouyang and W. Y. Ching, *Phys. Rev. B: Condens. Matter Mater. Phys.*, 2004, **70**, 155104.
21 O. Hochrein, R. Kniep and D. Zahn, *Chem. Mater.*, 2005, **17**, 1978.
22 D. Haverty, S. A. M. Tofail, K. T. Stanton and J. B. McMonagle, *Phys. Rev. B: Condens. Matter Mater. Phys.*, 2005, **71**, 094103.
23 W. T. Lee, M. T. Dove and E. K. H. Salje, *J. Phys.: Condens. Matter*, 2000, **12**, 9829.
24 M. R. T. Filgueiras, D. Mkhonto and N. H. de Leeuw, *J. Cryst. Growth*, 2006, **294**, 60.
25 P. Rulis, H. Z. Yao, L. Z. Ouyang and W. Y. Ching, *Phys. Rev. B: Condens. Matter Mater. Phys.*, 2007, **76**, 245410.
26 H. Chappell, M. Duer, N. Groom, C. Pickard and P. Bristowe, *Phys. Chem. Chem. Phys.*, 2008, **10**, 600.
27 R. Astala and M. J. Stott, *Phys. Rev. B: Condens. Matter Mater. Phys.*, 2008, **78**, 075427.
28 M. Corno, C. Busco, V. Bolis, S. Tosoni and P. Ugliengo, *Langmuir*, 2009, **25**, 2188.
29 R. Astala and M. J. Stott, *Chem. Mater.*, 2005, **17**, 4125.
30 R. Astala, L. Calderin, X. Yin and M. J. Stott, *Chem. Mater.*, 2006, **18**, 413.
31 S. Peroos, Z. Du and N. H. de Leeuw, *Biomaterials*, 2006, **27**, 2150.
32 K. Matsunaga, *J. Chem. Phys.*, 2008, **128**, 245101.
33 K. Matsunaga, H. Inamori and H. Murata, *Phys. Rev. B: Condens. Matter Mater. Phys.*, 2008, **78**, 094101.
34 K. Matsunaga and H. Murata, *J. Phys. Chem. B*, 2009, **113**, 3584.
35 N. H. de Leeuw, J. R. Bowe and J. A. L. Rabone, *Faraday Discuss.*, 2007, **134**, 195.
36 K. Matsunaga and A. Kuwabara, *Phys. Rev. B: Condens. Matter Mater. Phys.*, 2007, **75**, 014102.
37 D. Zahn and O. Hochrein, *J. Solid State Chem.*, 2008, **181**, 1712.
38 J. A. L. Rabone and N. H. de Leeuw, *Phys. Chem. Miner.*, 2007, **34**, 495.
39 N. L. Huq, K. J. Cross and E. C. Reynolds, *J. Mol. Model.*, 2000, **6**, 35.
40 X. Chen, Q. Wang, J. W. Shen, H. H. Pan and T. Wu, *J. Phys. Chem. C*, 2007, **111**, 1284.
41 H. Zhou, T. Wu, X. Dong, Q. Wang and J. W. Shen, *Biochem. Biophys. Res. Commun.*, 2007, **361**, 91.
42 X. L. Dong, Q. Wang, T. Wu and H. H. Pan, *Biophys. J.*, 2007, **93**, 750.
43 H. H. Pan, J. H. Tao, X. R. Xu and R. K. Tang, *Langmuir*, 2007, **23**, 8972.
44 J. W. Shen, T. Wu, Q. Wang and H. H. Pan, *Biomaterials*, 2008, **29**, 513.
45 H. P. Zhang, X. Lu, Y. Leng, L. M. Fang, S. X. Qu, B. Feng, J. Wng and J. X. Wang, *Acta Biomater.*, 2009, **5**, 1169.
46 N. Almora-Barrios and N. H. de Leeuw, *CrystEngComm*, 2010, **12**, 960.
47 A. Rimola, M. Corno, C. Zicovich-Wilson and P. Ugliengo, *J. Am. Chem. Soc.*, 2008, **130**, 16181.
48 N. Almora-Barrios, K. F. Austen and N. H. de Leeuw, *Langmuir*, 2009, **25**, 5018.
49 K. Makrodimitris, D. L. Masica, E. T. Kim and J. J. Gray, *J. Am. Chem. Soc.*, 2007, **129**, 13713.
50 M. Skepo, *J. Chem. Phys.*, 2008, **129**, 185101.
51 R. Bhowmik, K. S. Katti, D. Venna and D. R. Katti, *J. Mater. Sci.*, 2007, **42**, 8795.
52 R. Bhowmik, K. S. Katti and D. R. Katti, *J. Eng. Mech.*, 2009, **135**, 413.
53 R. Snyders, D. Music, D. Sigumonrong, B. Schelnberger, J. Jensen and J. M. Schneider, *Appl. Phys. Lett.*, 2007, **90**, 193902.
54 W. Y. Ching, P. Rulis and A. Misra, *Acta Biomater.*, 2009, **5**, 3067.
55 F. J. A. L. Cruz, J. N. C. Lopez, J. C. G. Calado and M. E. M. da Piedade, *J. Phys. Chem. B*, 2005, **109**, 24473.
56 F. J. A. L. Cruz, J. N. C. Lopez and J. C. G. Calado, *J. Phys. Chem. B*, 2006, **110**, 4387.
57 N. Y. Mostafa and P. W. Brown, *J. Phys. Chem. Solids*, 2007, **68**, 431.
58 F. J. Guild and W. Bonfield, *Biomaterials*, 1993, **14**, 985.
59 F. J. Guild and W. Bonfield, *J. Mater. Sci.: Mater. Med.*, 1998, **9**, 497.
60 I. Balac, P. S. Uskokovic, R. Aleksic and D. Uskokovic, *J. Biomed. Mater. Res.*, 2002, **63**, 793.
61 F. Wang, H. P. Lee and C. Lu, *J. Biomed. Mater. Res. A*, 2007, **80**, 146.
62 G. Thiagarajan, K. Deshmukh, Y. Wang, A. Misra, J. L. Katz and P. Spencer, *J. Biomed. Mater. Res. A*, 2007, **83**, 332.
63 P. Miranda, A. Pajares and F. Guiberteau, *Acta Biomater.*, 2008, **4**, 1715.
64 T. Van Cleynenbreugel, J. Schrooten, H. Van Oosterwyck and J. V. Sloten, *Med. Biol. Eng. Comput.*, 2006, **44**, 517.
65 S. Dyshlovenko, L. Pawlowski, B. Pateyron, I. Smurov and J. H. Harding, *Surf. Coat. Technol.*, 2006, **200**, 3757.
66 M. M. Branda, N. J. Castellani, R. Grau-Crespo, N. H. de Leeuw, N. C. Hernandez, J. F. Sanz, K. M. Neyman and F. Illas, *J. Chem. Phys.*, 2009, **131**, 094702.
67 R. Grau-Crespo, F. Cora, A. A. Sokol, N. H. de Leeuw and C. R. A. Catlow, *Phys. Rev. B: Condens. Matter Mater. Phys.*, 2006, **73**, 035116.
68 A. Ramraj, I. H. Hillier, M. A. Vincent and N. A. Burton, *Chem. Phys. Lett.*, 2010, **484**, 295.
69 K. M. Neyman and F. Illas, *Catal. Today*, 2005, **105**, 2.
70 C. R. A. Catlow, in *Computer Modelling in Inorganic Crystallography*, ed. C. R. A. Catlow, Academic Press, 1st Edition, 1997, (ch. 1), pp 1.
71 G. Kresse and J. Hafner, *Phys. Rev. B: Condens. Matter*, 1993, **47**, 558.
72 G. Kresse and J. Hafner, *Phys. Rev. B: Condens. Matter*, 1994, **49**, 14251.
73 G. Kresse and J. Furthmüller, *Phys. Rev. B: Condens. Matter*, 1996, **54**, 11169.
74 G. Kresse and J. Furthmüller, *Comput. Mater. Sci.*, 1996, **6**, 15.
75 D. Vanderbilt, *Phys. Rev. B: Condens. Matter*, 1990, **41**, 7892.
76 S. P. Bates, G. Kresse and M. J. Gillan, *Surf. Sci.*, 1998, **409**, 336.

77 J. P. Perdew, J. A. Chevary, S. H. Vosko, K. A. Jackson, M. R. Pederson, D. J. Singh and C. Fiolhas, *Phys. Rev. B: Condens. Matter*, 1992, **46**, 6671.
78 H. J. Monkhorst and J. D. Pack, *Phys. Rev. B: Solid State*, 1976, **13**, 5188.
79 G. W. Watson, E. T. Kelsey, N. H. de Leeuw, D. J. Harris and S. C. Parker, *J. Chem. Soc., Faraday Trans.*, 1996, **92**, 433.
80 W. Smith and T. R. Forester, *J. Mol. Graphics*, 1996, **14**, 136.
81 L. Verlet, *Phys. Rev.*, 1967, **159**, 98.
82 S. Nosé, *J. Chem. Phys.*, 1984, **81**, 511.
83 W. G. Hoover, *Phys. Rev. A: At., Mol., Opt. Phys.*, 1985, **31**, 1695.
84 M. Born and K. Huang, in *Dynamical Theory of Crystal Lattices*, Oxford University Press, Oxford, 1954.
85 B. G. Dick and A. W. Overhauser, *Phys. Rev.*, 1958, **112**, 90.
86 D. Mkhonto and N. H. de Leeuw, *J. Mater. Chem.*, 2002, **12**, 2633.
87 N. H. de Leeuw, *J. Phys. Chem. B*, 2004, **108**, 1809.
88 N. H. de Leeuw, *Phys. Chem. Chem. Phys.*, 2004, **6**, 1860.
89 P. Dauber Osguthorpe, V. A. Roberts, D. J. Osguthorpe, J. Wolff, M. Genest and A. Hagler, *Proteins: Struct., Funct., Genet.*, 1988, **4**, 31.
90 N. H. de Leeuw and J. A. L. Rabone, *CrystEngComm*, 2007, **9**, 1178.
91 A. S. Posner, A. Perloff and A. F. Diorio, *Acta Crystallogr.*, 1958, **11**, 308.
92 A. V. C. de Andrade, J. C. Z. da Silva, C. O. Paiva-Santos, C. Weber, V. H. dos Santos Utuni, S. M. Tebcherani, C. P. Ferreira Borges, E. da Costa and S. Martinez Manent, *Ceram. Eng. Sci. Proc.*, 2004, **25**, 639.
93 L. Stork, P. Mueller, R. Dronskowski and J. R. Ortlepp, *Z. Kristallogr.*, 2005, **220**, 201.
94 G. Renaudin, P. Laquerriere, Y. Filinchuk, E. Jallot and J. M. Nedelec, *J. Mater. Chem.*, 2008, **18**, 3593.
95 M. I. Kay, R. A. Young and A. S. Posner, *Nature*, 1964, **204**, 1050.
96 P. Fratzl, H. S. Gupta, E. P. Paschalis and P. Roschger, *J. Mater. Chem.*, 2004, **14**, 2115.
97 N. H. de Leeuw and J. A. Purton, *Phys. Rev. B: Condens. Matter Mater. Phys.*, 2001, **63**, 195417.
98 N. H. de Leeuw and T. G. Cooper, *J. Mater. Chem.*, 2003, **13**, 93.
99 N. H. de Leeuw, *Chem. Mater.*, 2002, **14**, 435.
100 M. E. Fleet, X. Liu and P. L. King, *Am. Mineral.*, 2004, **89**, 1422.
101 P. D. Moens, F. J. Callens, P. F. Matthys and R. M. Verbeeck, *J. Chem. Soc., Faraday Trans.*, 1994, **90**, 2653.
102 A. Kaflak-Hachulska, A. Samonson and W. Kolodziejski, *Calcif. Tissue Int.*, 2003, **73**, 476.
103 C. K. Loong, C. Rey, L. T. Kuhn, C. Combes, Y. Wu, S. H. Chen and M. J. Glimcher, *Bone*, 2000, **26**, 599.
104 E. F. Morgan, D. N. Yetkinler, B. R. Constantz and R. H. Dauskardt, *J. Mater. Sci.: Mater. Med.*, 1997, **8**, 559.
105 J. E. Harries, S. S. Hasnain and J. S. Shah, *Calcif. Tissue Int.*, 1987, **41**, 346.
106 H. M. Kim, K. Kishimoto, F. Miyaji and T. Kokubo, *J. Mater. Sci.: Mater. Med.*, 2000, **11**, 421.
107 J. C. Elliott, D. W. Holcomb and R. A. Young, *Calcif. Tissue Int.*, 1985, **37**, 372.
108 M. Okazaki, J. Takahashi, H. Kimura and T. Aoba, *J. Biomed. Mater. Res.*, 1982, **16**, 851.
109 J. Barralet, S. Best and W. Bonfield, *J. Biomed. Mater. Res.*, 1998, **41**, 79.
110 P. Moens, F. Callens, S. Van Doorslaer and P. Matthys, *Phys. Rev. B: Condens. Matter*, 1996, **53**, 5190.
111 S. J. Joris and C. H. Amberg, *J. Phys. Chem.*, 1971, **75**, 3172.
112 J. L. Meyer and B. O. Fowler, *Inorg. Chem.*, 1982, **21**, 3029.
113 N. H. de Leeuw, *Phys. Chem. Chem. Phys.*, 2002, **4**, 3865.
114 D. McLean, *Grain Boundaries in Metals*, Clarendon, Oxford, 1957.
115 R. Rohanizadeh, M. Trecant-Viana and G. Daculsi, *Calcif. Tissue Int.*, 1999, **64**, 430.
116 A. Wierzbicki and H. S. Cheung, *THEOCHEM*, 2000, **529**, 73.
117 V. K. Sharma, M. Johnsson, J. D. Sallis and G. H. Nancollas, *Langmuir*, 1992, **8**, 676.
118 M. E. Barbour, D. M. Parker, G. C. Allen and K. D. Jandt, *Eur. J. Oral Sci.*, 2003, **111**, 428.
119 S. Sarda, E. Fernandez, M. Nilsson, M. Balcells and J. A. Planell, *J. Biomed. Mater. Res.*, 2002, **61**, 653.
120 G. Williams and J. D. Sallis, *Biochem. J.*, 1979, **184**, 181.
121 W. P. Tew, C. Mahle, J. Benavides, J. E. Howard and A. L. Lehninger, *Biochemistry*, 1980, **19**, 1983.
122 Y. Suetsugu, Y. Takahashi, F. P. Okamura and J. Tanaka, *J. Solid State Chem.*, 2000, **155**, 292.
123 M. Vignoles, G. Bonel, D. W. Holcomb and R. A. Young, *Calcif. Tissue Int.*, 1988, **43**, 33.
124 D. U. Schramm, J. Terra, A. M. Rossi and D. E. Ellis, *Phys. Rev. B: Condens. Matter Mater. Phys.*, 2000, **63**, 024107.
125 W. E. Brown and L. C. Chow, *Annu. Rev. Mater. Sci.*, 1976, **6**, 213.
126 J. Sadlo, P. Matthys, G. Vanhaelewyn, F. Callens, J. Michalik and W. Stachowicz, *J. Chem. Soc., Faraday Trans.*, 1998, **94**, 3275.
127 B. H. Clarkson, J. S. Wefel and F. F. Feagin, *J. Dent. Res.*, 1986, **65**, 963.